GRAVITY EFFECT UNDER STEADY-STATE AND UNSTEADY-STATE CORE FLOODING AND CRITERIA TO AVOID IT

Ying Guo*, Victor Nilsen**, Frank Hovland***
* Rogaland Research, Stavanger, Norway
** Statoil, Stavanger, Norway
*** Rogaland Research, Bergen, Norway

Abstract Unsteady- or steady-state coreflooding in horizontal direction can be affected by gravity forces. Gravity segregation of the fluids will occur when the gravity force due to the density difference between the fluids used is comparable with the viscous forces under core flooding. When this happens the assumptions usually used for interpretation of the results will not be satisfied. This paper consists of a numerical simulation study based on the experimental data measured on a sample from the North Sea. The gravity segregated flow is confirmed by imaging using CT-scanning. A number of numerical simulations in 2-dim. mode have then been conducted with various flooding conditions in order to define a criterion for onset of gravity affected flow.

INTRODUCTION

Horizontal core flooding experiments are usually conducted following Rapoport and Leas[1] scaling rule ($qL\mu/A$ [=cp cm^2/min] > 1-5) defining a injection rate usually so high that the capillary effect can be ignored. Occasionally, lower flow rates are desired when conducting core flooding, for instance to match the real reservoir rate, or to avoid particle migration problems, etc. Low injection rate combined with high permeability of core sample, unfavourable mobility ratio and considerable density difference of the fluids give rise to gravity forces comparable with the viscous forces. Hence, a gravity affected flow inside the core will occur.

Craig et al.[2] measured the gravity segregation in frontal drives using scaled physical models. They found that for linear systems, the volumetric sweep efficiency at breakthrough can be correlated to a function of the ratio of viscous to gravity forces, namely:

$$\Delta P_g/\Delta P_V = q\mu L / K_X \Delta\rho g h A$$

where K_x is the horizontal permeability, $\Delta\rho$ the density difference between the phases, g the earth gravity acceleration, q the injection rate, μ the viscosity of the displacing phase, L, h and A the length, height and cross-section of the model. The lower this ratio, the more significant were the gravity effects.

Dombrowski and Brownell[3] presented a general correlation between residual wetting phase saturation and the sum of dimensionless viscous and gravitational forces causing desaturation. The dimensionless number they presented is the sum of the Capillary and Bond numbers. Capillary number is the dimensionless ratio of viscous to capillary forces. Bond number is the dimensionless ratio of gravitational to capillary forces.

Capillary Number: $N_C = u\,\mu / \sigma\cos\theta$

Bond Number: $N_B = K\,\Delta\rho\, g / \sigma\cos\theta$

where σ is the interfacial tension, θ the contact angle, and u the flow velocity.

In the present work, we define a segregation number by using the ratio between Bond number and Capillary number:

Segregation Number: $N_s = K\,\Delta\rho\, g / u\,\mu$

A number of simulation runs are made in both 1-dim. and 2-dim. mode based on experimental data. At otherwise identical conditions, we assume that the difference between the results from 2-dim. and 1-dim. simulation represent the contribution from gravity effect only. A normalized breakthrough production for unsteady-state flow can be used to characterize the degree of gravity effect:

Normalized breakthrough production:
$Q^*_{BT} = Q_{BT}$ (2D sim) / Q_{BT} (1D sim.)

where Q_{BT} is the production at breakthrough in fraction of porevolume.

This paper presents first the experimental data that the simulation model is built on. Then a number of simulations with different segregation numbers allow the construction of a segregation curve (Q^*_{BT} vs. segregation number) from which a criterion for onset of gravity affected flow is defined.

EXPERIMENTAL OBSERVATIONS

CT-scanning: All the tomographic scans were taken using a third generation X-ray computer tomographic scanner[4]. The details and principles of CT are described elsewhere[5, 6].

To further enhance the visualization of the fluid during the displacement, a base image is subtracted. The base image is taken immediately before the fluid injection in each experiment. Saturation and saturation changes can easily be obtained using the 2D-imaging by CT. The saturation distribution is used to detect fluid segregation.

Core sample: The core sample is homogeneous, with fairly high permeability (air permeability 4061 md). The capillary pressure curves for primary drainage, imbibition and secondary drainage are measured on an endcap by Hg-intrusion and retraction. The Hg-air capillary pressure is then scaled to obtain drainage oil-water capillary pressure curves needed in the simulations. The scaling parameters used are: Interfacial tension σ(Hg-air)=480 dyne/cm, σ(water-oil)=30 dyne/cm. Contact angle θ(Hg-air)=140°, θ(water-oil)=30°. For the imbibition process such scaling will only be correct for a strongly water-wet core. An artificial imbibition curve is used in the simulations since the core sample is from a reservoir which seems to behave as neutral to weakly water-wet. Relative permeability measured on a neighbouring core sample indicates an end-point value for water at S_{or} to be 0.34. This value has been used in the simulations. Burdine correlation[7] with a λ-value of 2.0 (giving a 4th order polynomial) is used to generate the relative permeability curves, both for the drainage and imbibition process. The rock and fluid data are summarized in Table 1. Table 2 shows the relative permeability and capillary pressure curves used in the simulation study.

Table 1: Rock and fluid properties

Core data:		Fluid Data	
Length:	5.07 cm	Water density:	1.027 g/cm^3
Diameter:	3.72 cm	Water viscosity:	1.06 cp
Area:	10.87 cm^2	Oil density:	0.742 g/cm^3
Porosity:	23.2 %	Oil viscosity:	1.3 cp
Air permeability:	4061 md		
Water permeability:	3760 md		

Table 2: Water-oil relative permeability and capillary pressure

1. drainage				Imbibition		
S_w	K_{rw}	K_{ro}	P_c	K_{rw}	K_{ro}	P_c
0,100	0,00000	1,00000	115,00			
0,200	0,00015	0,78036	25,00			
0,300	0,00243	0,57506	7,00			
0,312				0,00000	1,00000	0,500
0.360	0,00696	0,46347	3,90	0,00010	0,74462	0,100
0,400	0,01234	0,39506	3,10	0,00108	0,54803	0,020
0,500	0,03901	0,24767	2,20	0,02266	0,17949	0,000
0,600	0,09526	0,13656	1,88	0,12481	0,01935	0,000
0,700	0,19753	0,06172	1,75	0,34000	0,00000	0,000
0,800	0,36595	0,01950	1,66			
0,900	0,62429	0,00259	1,56			
0,960	0,83372	0,00017	1,30			
0,980	0,91403	0,00002	1,22			
1,000	1,00000	0,00000	0,00			

Unsteady-state flooding:

CT-images were taken perpendicular to the flow direction in order to observe how the saturation front is distributed. Such scanning technique also contributes to images with less geometrical distortions.

Primary drainage: The sample was 100% saturated with water containing sodium iodide to increase the CT-contrast between oil and water. Light refined oil was injected into the sample which was mounted in a Hassler core holder. The injection rate was kept constant at 400 cm^3/hour until the production ceased and a S_{wi} was established. Figure 1 shows the saturation distribution during primary drainage. As can be seen, changes in saturation first occur in the upper half, where the oil displaces the water. A short time later the saturation distribution becomes uniform over the whole cross section of the core sample.

Imbibition: Water was then injected into the sample to displace the oil at an injection rate of 170 cm^3/hour. The CT-scans were made 1.1 cm from the core inlet. Figure 2 shows the changes in saturation as water is injected into the core at S_{wi}. The saturation distribution shows a clear gravity effect. The water arrives first in the lower half and then continues to imbibe into the whole cross section. Despite the gravity segregation at the front, the final water saturation is distributed uniformly.

Steady-state flooding:

The gravity effect was then investigated for steady-state flooding on the same core. The displacement started at S_{wi} established by oil flooding. A constant total flow rate of 170 cm^3/hour was used. The water rate was increased in steps after equilibrium (no further change in differential pressure and saturation) was obtained at each step. The oil-water ratios used were 1.0/0.0, 0.9/0.1, 0.8/0.2, 0.5/0.5, 0.2/0.8, 0.0/1.0. Then the cycle was reversed, and the rate of water was decreased in steps with oil-water ratios of 0.2/0.8, 0.5/0.5, 0.8/0.2, 1.0/0.0. The fluids were injected into the core through a dual-tube end-piece. CT-scan was performed 1.2 cm from the core outlet. Figure 3 shows a series of saturation distributions at equilibrium at each step for the whole flooding cycle.

The saturation images clearly demonstrate that a phase separation has appeared at equilibrium. Water has a tendency to occupy the lower half of the core, while oil occupies the upper half. The segregation is most significant at the rate ratio of 0.5/0.5.

The question remaining unanswered was at which stage of the flooding process did the fluid segregation start and how did it develop. To investigate this, a longitudinal CT-view of the sample was taken during a new steady-state experiment at drainage mode with oil-water ratio of 0.5/0.5. The total flow rate was kept at 170 cm^3/hour. Figure 4 visualizes

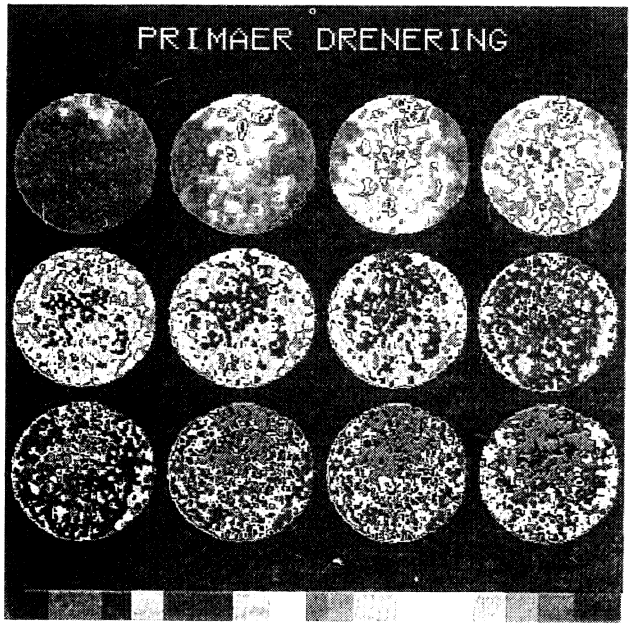

Figure 1: Primary drainage with q=400 cc/hour. CT-images taken at 1.1 cm from the inlet. The saturation scale increases from (S_{wi}) left to right (100%).

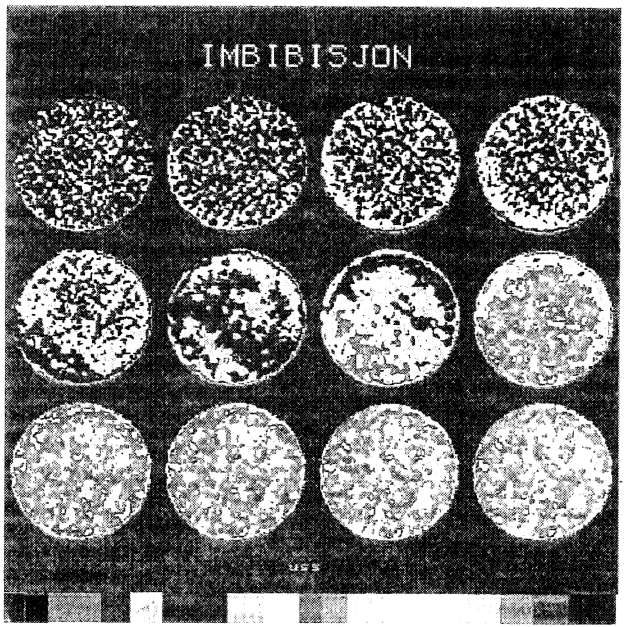

Figure 2: Imbibition with q=170 cc/hour. CT-images taken at 1.1 cm from inlet. The saturation scale increases from left (S_{wi}) to right (Sor).

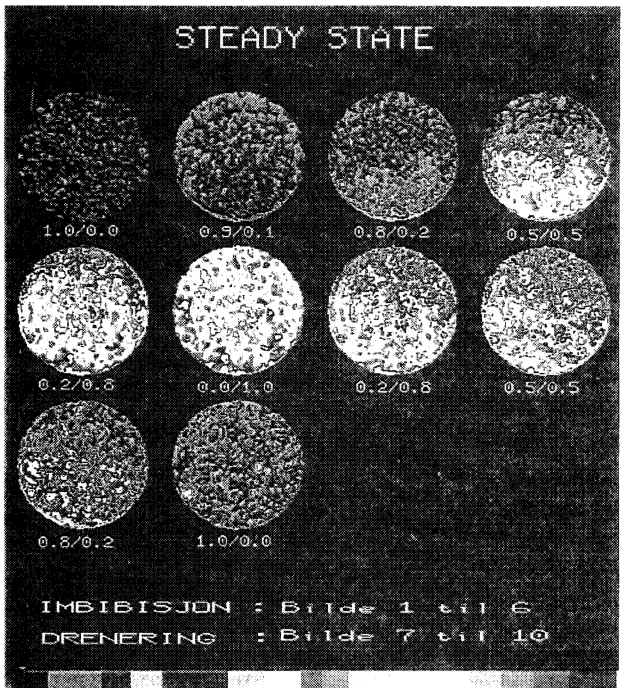

Figure 3:Steady-state images at equilibrium.
qt = 170 cc /hour. Imbibition cycle: Image 1 to 6. Drainage cycle: Image 7 to 10.

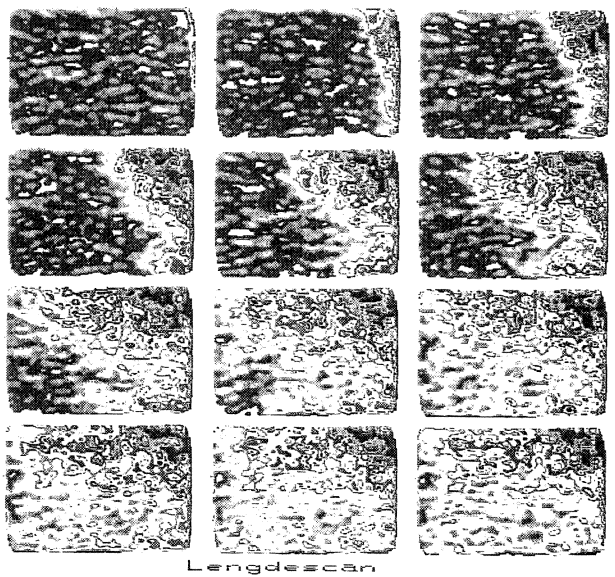

Figure 4:Steady-state flooding, CT-image in longitudinal direction. Oil/water ratio: 0.5/0.5. Start at S_{or}.

the phase separation along the core in the transition and equilibrium period. As one can see, the fluid separation is obvious already at the core inlet. Oil has a tendency to "climb up" into the upper half, and the final fluid distribution is clearly segregated.

NUMERICAL SIMULATIONS:

Numerical simulations were performed using a coreflood simulator CENDRA[8] in two-dimensional mode. X-direction is along the core while y-direction is in the vertical plane which is subjected to the earth's gravity. The block size in z-direction approximates a circular cross-section, as shown in Figure 5. A grid refinement by a factor of about 5 in x-direction was made to accurately simulate the inlet and outlet end-effect.

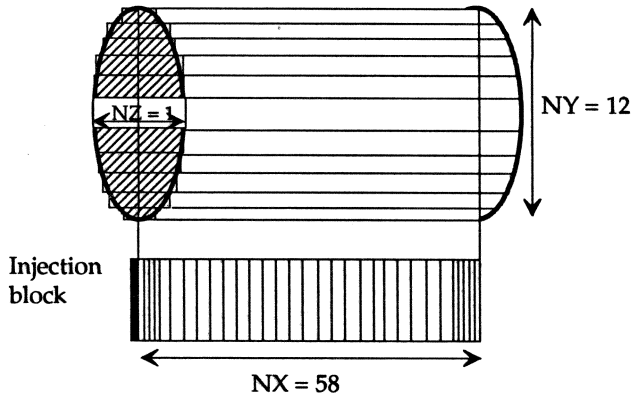

Figure 5: Grid system for simulations.

An injection block with small grid size is used at the injection face. It has zero capillary pressure, straight-line relative permeability curves and high absolute permeability. The purpose of this injection block is to simulate the end-piece with fluid distribution tracks in a certain pattern and to include the gravity term at the injection face.

Two injection strategies are used in the simulation runs for steady-state flooding. One is simultaneous injection of oil and water phase. With this injection strategy, both fluids are injected through the entire injection face with constant rate and at the specified rate ratio. This implies that the contact between the end-piece and the core inlet must be perfect, and that the fluid segregation occurs only after the fluids have entered the core

sample. The other strategy is separate fluid injection through two different grid blocks at the inlet end. Oil and water are separated until they enter the injection block where they are allowed to redistribute. This injection strategy simulates the dual-tube end piece used in the experiments.

Numerical dispersion is controlled using a relatively large number of grid blocks (NX=58) in x-direction. The number of grid blocks in y-direction is chosen to be 12 to compromise between CPU time and numerical dispersion. A number of simulation runs show that the numerical dispersion using this grid system, is negligibly small.

1-dim. simulations are made as reference to the 2-dim. simulations. They are performed with identical parameters except that the number of blocks in y-direction is 1.

SIMULATION RESULTS FOR UNSTEADY-STATE FLOODING:

Simulation runs of primary drainage and imbibition processes are performed with the same conditions as the experiments. Both primary drainage and imbibition show a slight tendency of gravity segregation at the fluid front. The segregation is minimal at the end of flooding. Figures 6 and 7 show the simulated saturation profiles in the transition period.

Simulation runs with injection rates ten times less than the real ones (400 cm^3/hour for primary drainage and 170 cm^3/hour for imbibition) are performed and the results are shown in Figures 8 and 9. These runs are significantly affected by gravity. Figure 10 shows the differential pressure and production curves for the imbibition flooding, from 2-dim. and 1-dim simulation where the gravity effect is not included. Note that the scale is enlarged to emphasize the part of interest. The comparison indicates an earlier breakthrough when gravity segregation occurs. The breakthrough does not correspond to the highest differential pressure point as normal and the differential pressure is generally lower. The latter effect will give an over-estimated relative permeability value.

A number of cases are simulated by changing the parameters to give different segregation numbers. The normalized breakthrough production as function of segregation number is presented in Figure 11 for primary drainage process, and Figure 12 for imbibition process. Tables 3 and 4 list the parameters changed in the simulation runs.

Figures 11 and 12 show a region with low segregation numbers where the segregation curve is relatively flat. In the region with large segregation numbers, the segregation curve decreases with a much steeper slope. The cross-over between these two regions falls at a segregation

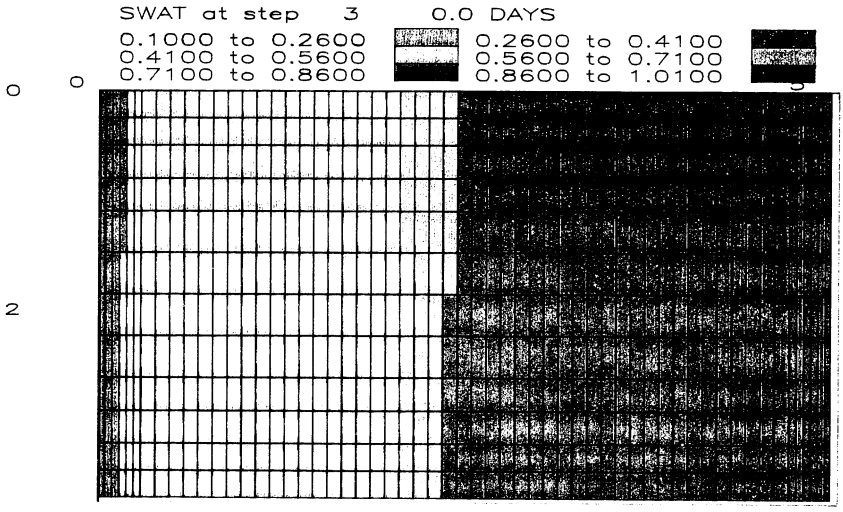

Figure 6: Unsteady-state flooding, primary drainage under experimental conditions.Simulated Sw-image at t = 0.5 min.. q = 400 cc/hour. Ns = 1.71 x 10^{-5}.

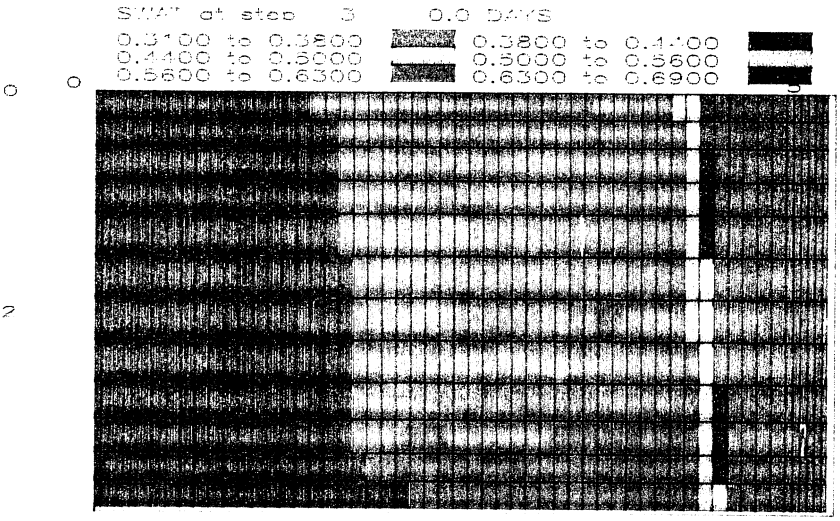

Figure 7: Unsteady-state flooding, imbibition under experimental conditions. Simulated Sw-image at t = 1.2 min.. q = 170 cc/hour. Ns = 2.28 x 10^{-4}.

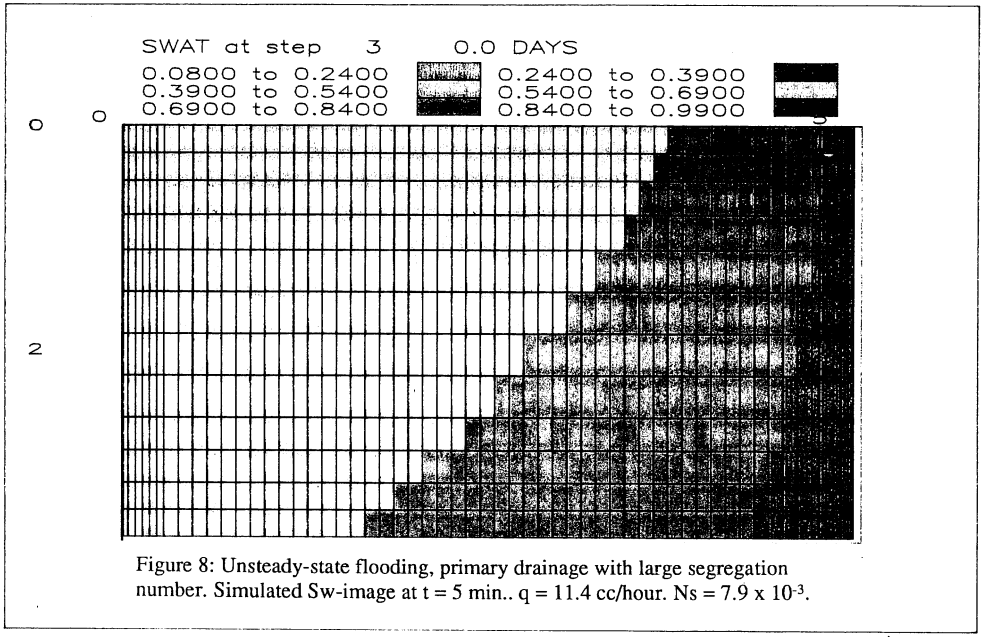

Figure 8: Unsteady-state flooding, primary drainage with large segregation number. Simulated Sw-image at t = 5 min.. q = 11.4 cc/hour. Ns = 7.9 x 10^{-3}.

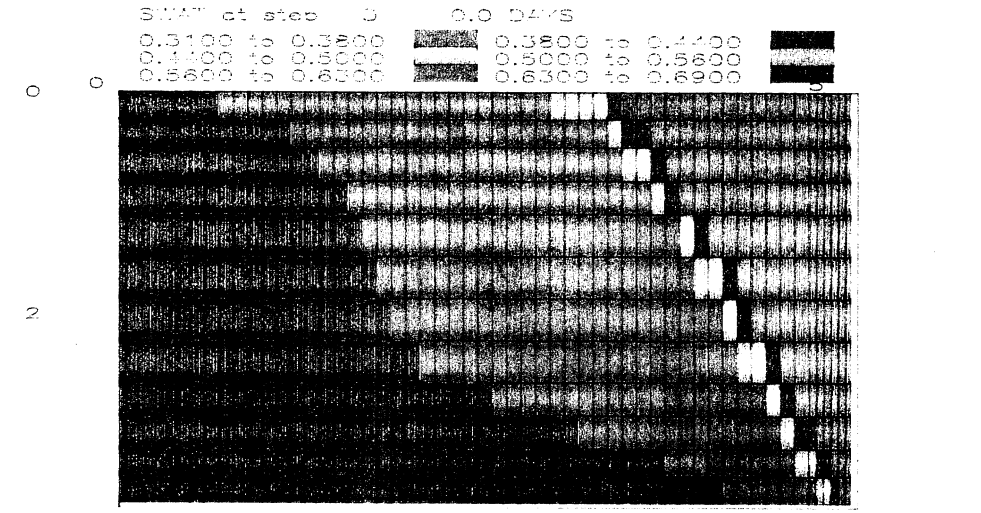

Figure 9: Unsteady-state flooding, imbibition with large segregation number. Simulated Sw-image at t = 12 min.. q = 17 cc/hour. Ns = 2.3 x 10^{-2}.

number of about 10^{-3}. This is true for both the imbibtion and primary drainage processes studied.

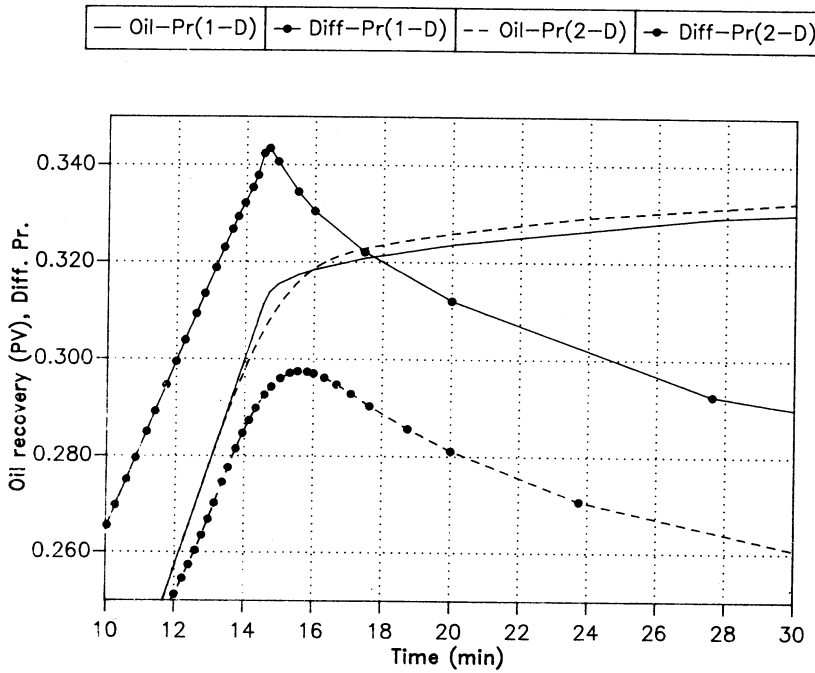

Figure 10: Comparison of differential pressure and oil recovery from 1-dim. and 2-dim. simulation. Unsteady-state imbibition with large segregation number. q=17 cc/hour, Ns=0.0023.

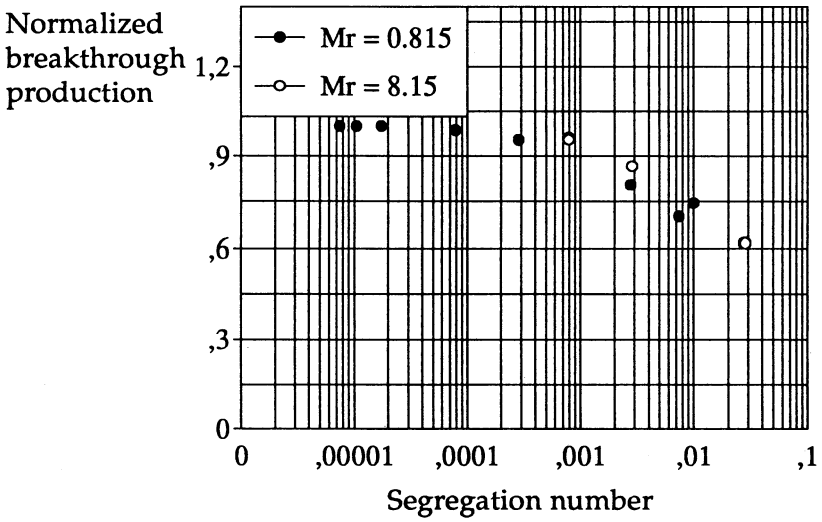

Figure 11: Normalized breakthrough production as function of segregation number, primary drainage. (Mr refers to mobility ratio).

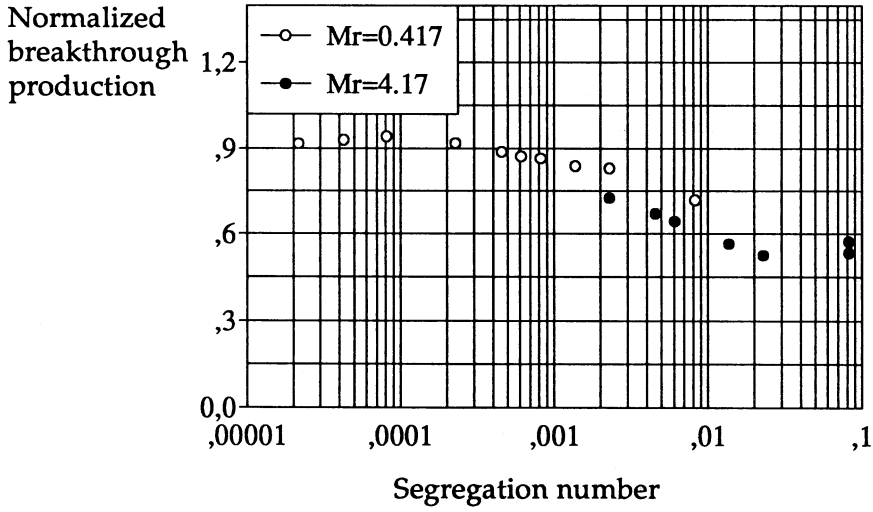

Figure 12. Normalized breakthrough production as function of segregation number, imbibition (Mr refers to mobility ratio).

Table 3: Parameters used in 2-dim.simulation, primary drainage

Run	ρ_o (g/cc)	μ_o (cp)	q (cc/min)	K (md)	Q_{BT} (f.PV)	Q^*_{BT} (f.PV)	N_S (x10^4)	qLμ/A *
1	1,000	1,30	6,667	3760	0,5202	1,0000	0,0749	4,043
2	0,742	1,30	6,667	500	0,5592	1,0000	0,1051	4,043
3	0,742	6,0	6,667	3760	0,6286	0,9998	0,1714	18,66
4	0,742	1,30	6,667	3760	0,5222	0,9875	0,7910	4,043
5	0,001	1,30	6,667	3760	0,5043	0,9547	2,8475	4,043
6	0,742	1,30	0,667	10000	0,3878	0,9620	7,9063	0,405
7	0,742	1,30	0,1905	3760	0,2999	0,8058	27,682	0,116
8	0,742	1,30	0,1905	10000	0,2220	0,7020	73,624	0,116
9	0,001	1,30	0,1905	3760	0,2357	0,7454	99,656	0,116
10	0,742	0,13	6,667	3760	0,3250	0,9556	7,9099	0,404
11	0,742	0,13	6,667	3760	0,2950	0,8663	28,475	0,404
12	0,001	0,13	0,667	3760	0,1525	0,6200	284,63	0,040
13	0,742	0,13	0,1905	3760	0,1215	0,6179	276,82	0,012

ρ_w = 1.027 g/cc, μ_w = 1.06 cp *) = cp cm^2/min

$K_{rw}(S_w=1)$ = 1,00, $K_{ro}(S_{wi})$ = 1.0

Table 4: Parameters used in 2-dim.simulation, imbibition.

Run	ρ_o (g/cc)	μ_w (cp)	q (cc/min)	K (md)	Q_{BT} (f.PV)	Q^*_{BT} (f.PV)	N_S (x10^4)	qLμ/A *
1	1,000	1,06	2,833	3760	0,3081	0,9169	0,2162	1,40
2	0,742	1,06	2,833	700	0,3125	0,9303	0,4250	1,40
3	0,742	3	2,833	3760	0,3281	0,9420	0,8066	3,96
4	0,742	1,06	2,833	3760	0,3090	0,9196	2,2829	1,40
5	0,742	1,06	1,4165	3760	0,2975	0,8864	4,5658	0,70
6	0,742	1,06	2,833	10000	0,2920	0,8698	6,0716	1,40
7	0,001	1,06	2,833	3760	0,2903	0,8640	8,2185	1,40
8	0,742	1,06	0,472	3760	0,2807	0,8366	13,702	0,23
9	0,742	1,06	0,2833	3760	0,2785	0,8303	22,829	0,14
10	0,742	1,06	0,0786	3760	0,2407	0,7180	82,283	0,04
11	0,742	0,106	2,833	3760	0,2129	0,7234	22,829	0,14
12	0,742	0,106	1,4165	3760	0,1967	0,6676	45,658	0,07
13	0,742	0,106	2,833	10000	0,1886	0,6408	60,715	0,14
14	0,742	0,106	0,472	3760	0,1660	0,5648	137,02	0,023
15	0,742	0,106	0,2833	3760	0,1543	0,5261	228,29	0,014
16	0,001	0,106	2,833	3760	0,1570	0,5352	821,85	0,014
17	0,742	0,106	0,0786	3760	0,1678	0,5729	822,83	0,004

ρ_w = 1,027 g/cc, μ_o=1.3 cp *) = cp cm^2/min

$K_{rw}(S_{or})$=0.34, $K_{ro}(S_{wi})$=1.0

SIMULATION RESULTS FOR STEADY-STATE:

Attempts to reproduce the experimental observations failed with the simultaneous injection strategy. No significant fluid segregation could be observed using the experimental conditions. However, using the separate injection strategy which best simulates the dual-tube end-piece at inlet, the gravity segregation is clearly revealed. Figures 13 shows the simulation results. One simulation run with a rate ratio of 50/50, but ten times lower injection rate (17 cc/hour) is performed, and the result is shown in Figure 14.

No systematic simulation study with varying segregation number is performed for steady-state flooding. This is mainly due to the dependency of fluid segregation on shape of the relative permeability curves, a fact that has been confirmed in our considerable number of simulations. The degree of gravity segregation varies with different injection ratios. Thus it is necessary to define a new parameter in order to characterize the degree of segregation. We observed that the average saturation, even at severe segregation, is not much different from that without segregation. However, the differential pressure at equilibrium is lower for gravity affected flow. This will give over-estimated relative permeability values.

DISCUSSION

The criterion for onset of gravity affected flow is based on the rock system studied. Only the parameters included in the segregation number are systematically varied. In addition to these parameters, however, the capillary pressure and relative permeability curves are the other important factors that govern the flow process.

Various λ-values have been used to examine the shape effect of the relative permeability curves. It is found that higher λ-values, giving straighter relative permeability curves, will result in lower viscous forces, thus enhancing gravity segregation.

Simulation runs with ten times higher capillary pressure values at high segregation numbers have been conducted. The results show little effect on the gravity segregation, only on the front saturation gradient.

The core length is not included in the segregation number. Neither the shape of the capillary pressure curve, nor the saturation at which capillary pressure reaches zero has been studied. These are important factors that affect breakthrough production, and the criterion for onset of gravity affected flow. A segregation number that includes the above

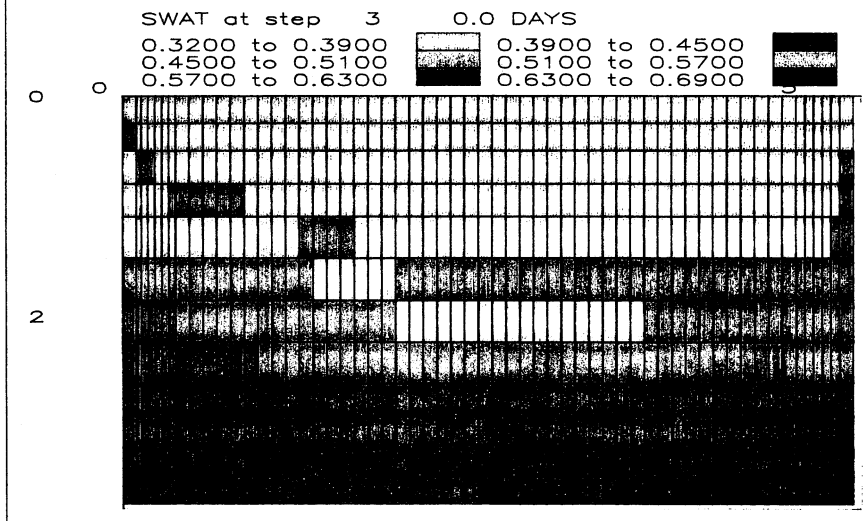

Figure 13: Steady-state flooding, imbibition with experimental conditions. Separate fluid injection. qt = 170 cc/hour. Oil-water ratio: 0.5/0.5.

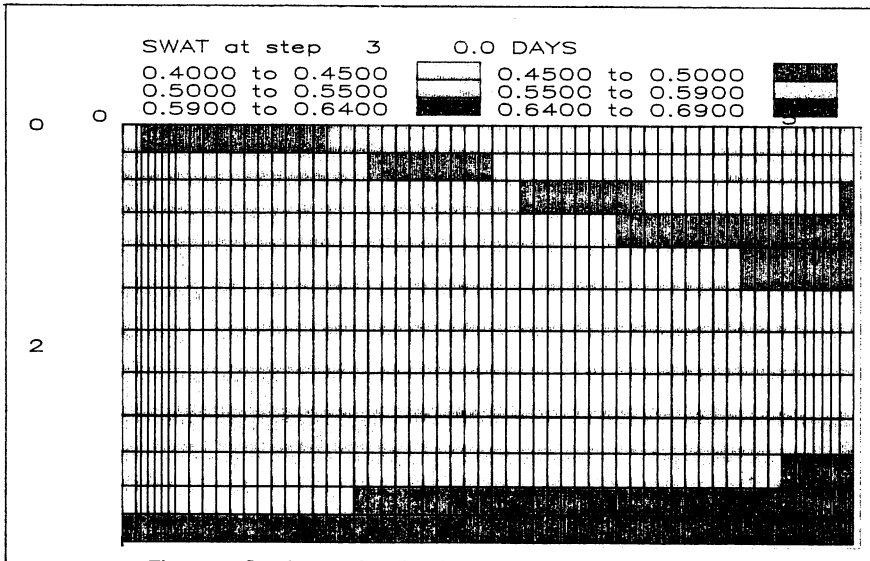

Figure 14: Steady-state flooding, imbibition with large segregation number. Simultaneous fluid injection. qt = 17 cc/hour. Oil-water ratio: 0.5/0.5.

mentioned factors might be necessary in order to establish a more robust criterion for onset of gravity affected flow.

Some of the simulated cases violate Rapoport and Leas' scaling law[1] for neglecting capillary effect (ref. the last column in Tables 3 and 4). However, the 1-dim. simulation runs show that the breakthrough production is only dependent on the change of mobility ratio, not the injection rate. This indicates that the system studied is not subjected to the capillary effect even at very low scaling factors. This also reminds us that the scaling law is not generally applicable without including mobility ratio and a measure of capillary force.

CONCLUSIONS

1) The CT-scanning technique has been used to distinguish between viscous / capillary and gravity affected flow.

2) Gravity affected flow has been shown to exist by 2-dim. numerical simulations.

3) A criterion for onset of gravity segregated flow has been found for the rock system studied. This criterion is represented by a segregation number of 10^{-3} for unsteady-state flooding.

4) For steady-state flooding, effective and complete distribution of both fluids at inlet is essential. Whenever this is satisfied, the influence of gravity at equilibrium with a segregation number less than 10^{-3}, is of less importance on the core length studied.

ACKNOWLEDGEMENTS:

The authors wish to acknowledge J.E. Nordtvedt, S.L. Tonstad, A. Hove and J.K. Ringen who have performed the experimental work. We also thank both Rogaland Research and Statoil for permission and support to publish this paper.

REFERENCES

1). Rapoport L.A. and Leas, W.J.: "Properties of Linear Waterflood Behaviour and End Effects in Water-Wet Porous Media", TRANS AIME 198, 1953, pp139-148.
2). Craig, F.F., Jr, Sanderlin, J.L., Moore, D.W. And Geffen, T.M.: " A Laboratory Study of Gravity Segregation in Frontal Drive"; TRANS. AIME, 1957, Vol.210, pp. 275-282.
3). Dombrowski, H.S. and Brownell, L.E.: "Residual Equilibrium Saturation of Porous Media", Ind.Eng.Chem. (1954) pp.1207-1219.
4). Hove, A.O, Nilsen V. and Leknes, J.: "Visualization of Xanthan Flood Behaviour in Core Samples by Means of X-Ray Tomography", SPERE, (Nov.1990) pp 475-480.
5). Hove, A.O., Ringen J.K. and Read, P.: "Visualization of Laboratory Corefloods with the Aid of Computerized Tomography of X-rays", SPERE (May 1987) pp 148-54.
6). Wellington, S.L. and Vinegar, H.J.: "X-Ray Computerized Tomography", JPT (Aug.1987) pp 885--98
7). Burdine, N.T.: "Relative Permeability Calculations from Pore Size Distribution Data", TRANS AIME 198 (1953) pp.71-78.
8). Guo, Y.: "Simulator CENDRA", Report No.44, 1986, Rogaland University Centre.